Granular scaling laws for helically driven dynamics

Andrew Thoesen , Teresa McBryan, Darwin Mick , Marko Green, Justin Martia, and Hamid Marvi[*]

School for Engineering of Matter, Transport, and Energy, Arizona State University, Tempe, Arizona, 85287

Exploration of granular physics for three-dimensional geometries interacting with deformable media is crucial for further understanding of granular mechanics and vehicle-terrain dynamics. A modular screw propelled vehicle is, therefore, designed for testing the accuracy of a novel helical granular scaling law in predicting vehicle translational velocity and power. A dimensional analysis is performed on the vehicle and screw pontoons. Two additional pontoon pairs of increased size and mass are determined from dimensional scalars. The power and velocity of these larger pairs are predicted by the smaller pair using the scaling relationships. All three sets are subjected to ten trials of five angular velocities ranging from 13.7 to 75.0 revolutions per minute in a high interlock lunar regolith analog derived from mining tailings. Experimental agreement for prediction of power (3–9% error) and translational velocity (2–12% error) are observed. A similar set of geometries is subjected to multibody dynamics and discrete element method cosimulations of Earth and lunar gravity to verify a gravity-dependent subset of the scaling laws. These simulations show agreement (under 5% error for all sets) and support law validity for gravity between Earth and lunar magnitude. These results support further expansion of granular scaling models to enable prediction for vehicle-terrain dynamics for a variety of environments and geometries.

I. INTRODUCTION

Screw-propelled vehicles have been investigated for use on Earth in marshes [1], mud [2], lake shores [3], and icy or snowy [4] environments. Mobility in various deformable environments, coupled with kinematic simplicity, makes screw propulsion a potential solution for exploratory space vehicles in granular environments with high slip. Helical propulsion for a single helix has been previously investigated in the context of geometry, granular confinement, and external load [5]. Such propulsion is driven by the asymmetrical shape of such a helix. A second study [6] examined geometry of helix angle, length, diameter, and differences in media performance. Similarly, helical propulsion in different fluids, in the context of micro-organism motion, has also been examined [7,8]. However, all studies examined a fully submerged single slender-bodied helix rather than the surface mobility of dual helicoid screw pontoons in a granular deformable environment.

The early precedent for granular mechanics as a field favoring empirical or semiempirical approaches, including for lunar mobility [9], was established by Bekker [10]. Advancements [11] in examining many different soil-geometry models, including those with gravity variation, followed. This is important because weight-offset testing can have erroneous or opposite results compared to identical experiments in gravity-varied parabolic flight testing [12] due to the gravitational compaction of grains. Recent years have seen a more

theoretical shift towards understanding the physics of granule-geometry interaction. One example is granular resistive force theory (RFT), an examination of granular material reactions [13–19] driven by assumptions similar to fluid resistive force theory. In the empirical model of granular RFT, an experimental calibration procedure examines the force resistance (with vertical and translational components) on a plate. The plate intrudes into a target medium at constant speed in different combinations of plate orientation angle and velocity vector. This produces a characteristic response for the medium as a function of the variable pair (plate angle and velocity angle). An arbitrary intruder of interest can then be modeled as a rigid body approximated by individual plate elements. Under the assumption of superposition, each plate element resistance can be calculated as a function of depth, orientation, and velocity, then, summed linearly whereas assuming the media is nondeforming and isotropic. This has shown itself to be a good approximation for a variety of experiments and shapes and have sound theoretical basis [18,20,21]. However, the force generated by multiple windings in screw blades submerged in granular media has previously been shown to not adhere to linear superposition in this manner [22]. Observations about the granular material itself and its flowability (to be discussed in subsection Experimental Design and Setup) also raised the issue of possible difficulties. Because of this, other methods were sought.

RFT has been recently reconciled with other theoretical granular physics by assuming the target environment to be a continuum obeying a frictional yield criterion without cohesion [23–25]. Both RFT and continuum approaches can be explained by "frictional plasticity" theories [20] and are hypothesized to handle colloidal deformable environments, such

_____
[*]hmarvi@asu.edu

as muds and gels. A comparison of dimensional analyses of both approaches resulted in the same set of scaling parameters [26]. This led to a set of predictive granular scaling laws (GSLs) for wheeled locomotion in granular media. These have also been comparatively tested with the new material point method [27], a computational approach similar to finite element methods. Nonetheless, none of the above laws address screw helicoid propulsion.

Motivated by the desire to explore the physics of helical geometries in granular media, we derived a new set of scaling laws for granular locomotion driven by screw shapes using dimensional analysis. Although the same mechanisms related to granular plasticity are assumed, it was inconclusive whether three-dimensional force tensors on the geometry would resolve in practice in the same manner as the pseudo-two-dimensional vectors previously studied in GSL. These helical granular scaling laws (HGSLs) complement the wheeled granular scaling laws. We show through theory, experiment, and simulation that the deformation mechanics of three-dimensional screw-driven mobility in granular media results in comparable power and velocity scaling predictions to those produced by wheeled scaling laws. We evaluate a set of three screws with increasing size and mass based upon HGSL in a crushed basalt lunar regolith analog derived from mining tailings. The power and velocity results of these sets are analyzed and the predictability of HGSL is assessed. Lunar gravity is, then, investigated through multibody dynamics and discrete element method (MBD-DEM) cosimulations with geometries identical to experiments. The results have implications for lunar mobility as well as agriculture, mining, and other Earth industries.

II. METHODS AND MATERIALS

A. Dimensional analysis of helical propulsion in granular media

Most granular mechanics and vehicle modeling with deformable media involving wheels share a fundamental assumption: the depth invariance of the wheel shape. Often, the geometry is assumed constant through the entire thickness of the wheel, reducing the effective stress fields analyzed to two dimensional. This does not hold for a rotating three-dimensional helical geometry as seen in Fig. 1.

Instead, a few alternative assumptions are applied to constrain the problem. We explicitly limit the helicoid shape of the screw pontoon to be radially constant; that is, a slice of the geometry should be identical to any other portion but for a rotational offset. The screw pontoon radii are constant throughout the geometry; i.e., the pontoon itself does not taper, and the blade radii do not vary. Finally, similar to wheels, we design a long enough distance between pontoons to negate any interactive effects between the two granular flows. In the environment, we assume the screw moves through non- or weakly cohesive granular media expressed as a frictional continuum. Drag is neglected (this will be discussed with results), and friction is assumed rate independent. We assume sufficient distance from container walls to avoid boundary effects [28] and sufficient depth of engagement (greater than five to ten grain diameters [29]) to model the environment as one continuous block with constant internal friction and
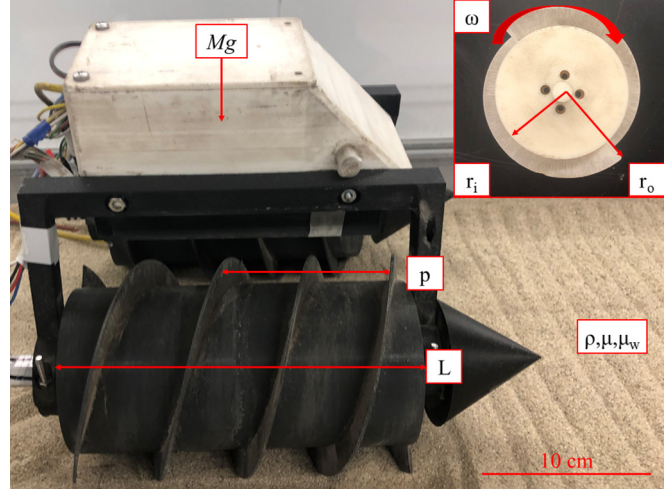

FIG. 1. Side view of the vehicle and screw pontoon with top view of screw pontoon inset. All HGSL parameters labeled.

properties. If the geometry and environment are held to these relationships, the power and translational velocity of the vehicle can be expressed as

$$[P, V] = f(p, r_i, r_o, l, m, \omega, \rho, \mu, \mu_s, g, t). \quad (1)$$

The screw geometry is described by the characteristic pitch p, its inner radius r_i, its outer radius r_o, and its length l. The system is described by its total mass m and a driving angular velocity ω with the axis of rotation parallel to the direction of travel. The environment is described by gravity g and the granular characteristics ρ, μ, and μ_s; these are the granular density, internal friction, and screw-grain friction, respectively. The granular characteristics are assumed constant and occur as a function of the granular environment and its interaction with the geometry. Time t is the last driving parameter. Our target outputs are power P and translational velocity V. We nondimensionalize by

$$L = p, \quad M = m, \quad T = \sqrt{\frac{p}{g}}. \quad (2)$$

We then express all variables in terms of their dimensions and create dimensionless groups. To create the dimensionless group, we multiply it by our variable choices in such a way that these units cancel out,

$$\bar{\rho} = \rho * \frac{L^3}{M} = \frac{\rho p^3}{m}. \quad (3)$$

This is performed with all variables until we produce a new function as follows:

$$\left[\frac{P}{mg\sqrt{pg}}, \frac{V}{\sqrt{pg}} \right] = \phi\left(\frac{r_i}{p}, \frac{r_o}{p}, \frac{l}{p}, \frac{\rho p^3}{m}, \mu, \mu_s, \frac{g}{p\omega^2}, t\sqrt{\frac{g}{p}} \right). \quad (4)$$

To simplify these laws, we make several additional assumptions:

(1) The nondimensional power and velocity should only be a function of the ratio of length and mass. We constrain both variables such that the ratio l/m is constant between pairs. To achieve this constraint, the expressions $\frac{l}{p}$ and $\frac{\rho p^3}{m}$ are

no longer independent. Instead, they are combined into one term as their product $\frac{\rho l p^2}{m}$. A similar assumption is implied in the original laws for wheels as well.

(2) We assume that the granular environment is constant between experiments with different pontoons. This implies a deep enough sinkage to eliminate any difference from surface effects between experiments as shallow sinkage has caused scaling laws to deviate in a previous study [29,30]. The dimensionless friction coefficient of grain-screw interaction, the internal friction of the granular media, and the expression for granular density are assumed constant; therefore friction and density are absorbed into the function ϕ.

(3) We assume constant gravity. This assumption will be later relaxed as we explore MBD-DEM simulations of a gravity-dependent nature, but for now it is absorbed into the function ϕ.

(4) We observe that, although power and velocity are a function of time, we are concerned with the comparison of steady state performance between vehicles and not with time-dependent characteristics. If we assume time-averaged steady state values, then, we eliminate time as a functional concern. Note that this is retained inside the functional expression, but all references to power and translational velocity, henceforth, refer to their steady state time-averaged values.

Thus, the final function is as follows:

$$\left[\frac{P}{m\sqrt{p}}, \frac{V}{\sqrt{p}}\right] = \Phi\left(\frac{r_i}{p}, \frac{r_o}{p}, \frac{lp^2}{m}, \frac{1}{p\omega^2}, t\sqrt{\frac{1}{p}}\right). \quad (5)$$

The result of this exercise is a dimensionless expression which looks similar to the original wheeled granular scaling theory [26] but for a screw in which the axis of rotation is parallel to the direction of travel. If we change our characteristic pitch p by some scalar a, change mass m by b, and constrain our remaining variables such that the values inside the function always remain constant, then, the value of Φ itself will remain identical. This implies that the power and velocity relationship between two sets of screws is a predictable ratio subject to scalars a, b. Given the above assumptions and two experiments, one with the inputs of $(p, m, r_i, r_o, l, \omega)$ and the other scaled by positive scalars a, b with inputs $(p', m', r_i', r_o', l', \omega') = (ap, bm, ar_i, ar_o, ba^{-2}l, a^{-1/2}\omega)$, the time-averaged powers and translational velocities are expressed as follows:

$$P' = ba^{1/2}P, \quad V' = a^{1/2}V, \quad (6)$$

where P' and V' are predicted from the designed scalar a, b differences between sets and the experimentally determined power and velocity of the smaller vehicle.

B. Experimental design and setup

The craft platform for these tests, seen in Fig. 1, consists of a central body with electronics located internally, a weight carrier to modify total craft mass, screw pontoons designed according to our HGSL function, two internal motors to drive the pontoons, and nose cones to reduce significance of any occurring front drag. Care was taken to avoid drag as much as possible and to avoid wall boundary effects by placing the craft pontoons at a minimum distance from the wall of
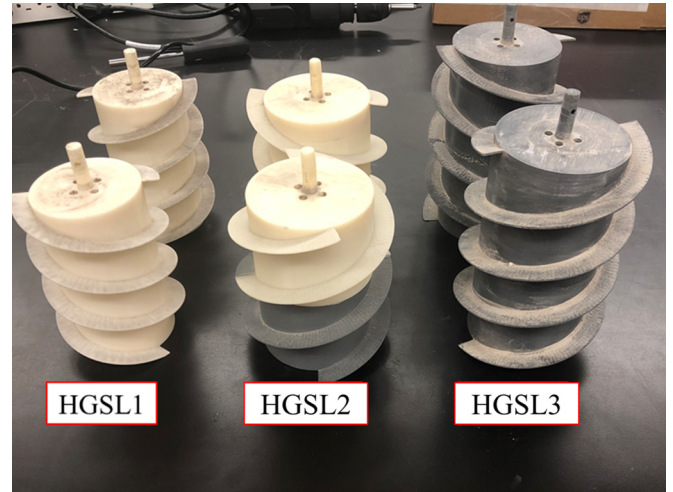

FIG. 2. Three different pontoons used in experiments. The parameters for HGSL1, HGSL2, and HGSL3 pairs can be found in Table I.

several hundred times the average particle size; no reaction was observed between the grains and the wall. To design a scaled experiment, we created three sets of screw pontoons seen in Fig. 2. HGSL1 is the label given for our base screw pontoon, and HGSL2 and HGSL3 are affected by the (a, b) scalar pair of (1.2, 1.44) and (1.2, 1.85), respectively. These scalar pairs are the ratios of pitch p and mass m, respectively, as seen in the relationships for Eq. (6). For example, HGSL2's pitch is $\times 1.2$ HGSL1's pitch, and its mass is $\times 1.44$ that of HGSL1.

The power and velocity of HGSL1 are experimentally determined. Then, the P', V' of either HGSL2 or HGSL3 are predicted from the scalar pair and HGSL1 P, V. Finally, these predictions are compared to the HGSL2 or HGSL3 experimental results. The choice of screw sizes and craft masses were based upon preliminary experiments which indicated the range of output power for our motors could be roughly doubled from the HGSL1 sizing. Therefore, HGSL2 was designed to require 157% of the power requirement for HGSL1. HGSL3 was designed for 203% of the power required for HGSL1. The chosen parameters for the experiments are listed in Table I. Trials were run as close to target revolutions per minute (RPM) as possible for HGSL1, HGSL2, and HGSL3. The five angular velocities of HGSL1 dictated the exact targets for HGSL2 and HGSL3, and the power at those velocities was, then, estimated based on a linear regression through the HGSL2 and HGSL3 points with the exact values at the required RPM extracted.

The granular material used in these experiments is a lunar analog named Black Point 1 (BP-1). This material shares close characteristics to a lunar regolith as fully detailed in a geotechnical assessment [31] and has been used extensively for lunar robotics testing [32,33]. It is a repurposed mining tailing composed of primarily crushed basalt. There are several important characteristics of BP-1 highlighted for the purposes of this paper, found in Suescun-Florez *et al.* unless otherwise noted:

TABLE I. Parameters chosen for helical pontoons.

Design	Pitch	Mass	Length	r_i	r_o	Target ω (RPM)
HGSL-1	7.5	1.441	14	3.75	5	15.0, 30.0, 45.0, 60.0, 75.0
HGSL-2	9.0	2.075	14	4.50	6	13.7, 27.4, 41.0, 54.8, 68.5
HGSL-3	9.0	2.666	18	4.50	6	13.7, 27.4, 41.0, 54.8, 68.5

(1) Particle size distribution tests show similar physical behavior to that of lunar regolith samples and other lunar simulants, such as JSC-1A [34]. The tests also show similar particle size distribution to other lunar simulants and within one standard deviation of lunar regolith samples (similar to other simulants). BP-1 is classified as a silty sand with a D60 value of 0.11 mm and a D30 value of 0.055 mm; 60% of particle sizes are finer (smaller) than 110 μm and 30% smaller than 55 μm.

(2) Scanning electron microscope images of BP-1 lead to classification of particle shape in the angular to subangular category and generally high elongation.

(3) The peak of principal stress ratio increased significantly with density, similar to JCS-1. The internal angle of friction was observed to significantly increase with relative density (D_r), showing 39° at 50% D_r and 51° at 85% D_r.

(4) BP-1 showed negligible (0–2 kPa) cohesion. Note that cohesion, in the strict sense, means the particles are able to support states of pure tension. However, the above characteristics microscopically lead to high friction granular interlock; this leads to macroscopic behaviors consistent with apparent cohesion, such as high trenching [35].

These specific aspects of BP-1 differentiate it from other granular media frequently used to study granular mechanics, such as poppy seeds, silica and quartz sands, glass beads, or plastic beads. Performing scaling experiments with a lunar simulant provides an opportunity to explore scaling models with a complex media. It also will help determine whether these techniques may be suitable when designing vehicles for lunar terrain. The distinct macroscopic behavior of lunar regolith and simulants from highly flowable media, such as poppy seeds or silica sands is of significance for this matter. Earth testing of Mars Curiosity Rover traversability shows the variability in performance and interactions with different types of granular environments [36]. This variability indicates that evaluation of generalized laws in a material close to target environment is valuable.

Experiments were performed in the simulant containment unit seen in Fig. 3. The BP-1 was tilled by a thatch rake to prevent large stress concentrations. The craft was placed on top of the BP-1 at one end of the chamber. Each trial ran from one end of the chamber to the other. Camera location and settings were kept constant between all trials. Using a MATLAB-based color tracking program, position versus time was determined and analyzed for each video. Mechanical power was evaluated using in-line Hall-effect current sensors, located immediately before the motor, to obtain individual current readings. The current was converted to torque by the given motor constant, and the time-averaged torque and angular speed were multiplied during the steady state regime to produce time-averaged power. Three screw pontoons were run for ten trials at five target speeds (150 total trials) with angular

velocity ω' prescribed by the set of parameters for Eq. (6). The results of the ten trials for each data point were averaged, and the standard error was calculated.

III. RESULTS AND DISCUSSION

A. Power and velocity predictions for HGSL experiments

The results of the comparison between predicted mechanical power and actual mechanical power indicate that the laws provide a reasonable estimate in BP-1 [Fig. 4(a)]. The black lines shown on the graphs indicate the line of perfect prediction when actual power and predicted power coincide. The error of HGSL2 ranged from −3% to 4%; the slower speeds were slightly underpredicted, and the higher speeds were overpredicted. HGSL3 showed the opposite trend; it had power prediction errors ranging from −4% to 9%. The standard errors for HGSL2 and HGSL3 are noted by the vertical bars and are not visible for many of the lower speeds due to the generally high precision in those datasets. Note that, although differences between predicted power and actual power increased with power magnitude, the actual error percentage was not observed to correlate with an increase with power.

The results of the comparison between predicted velocity and actual velocity indicate the laws provide a reasonable velocity estimate in BP-1 as well [Fig. 4(b)]. The HGSL2 error ranged from 2 to 12% without angular velocity dependence and with all values above predicted. The HGSL3 error ranged from −4% to 6% error with slower trials lower than predicted and faster trials higher than predicted. One observation made during experiments was the existence of a small amount of granular accumulation in front of all three sets. It is possible that the HGSL3 set with higher mass required additional
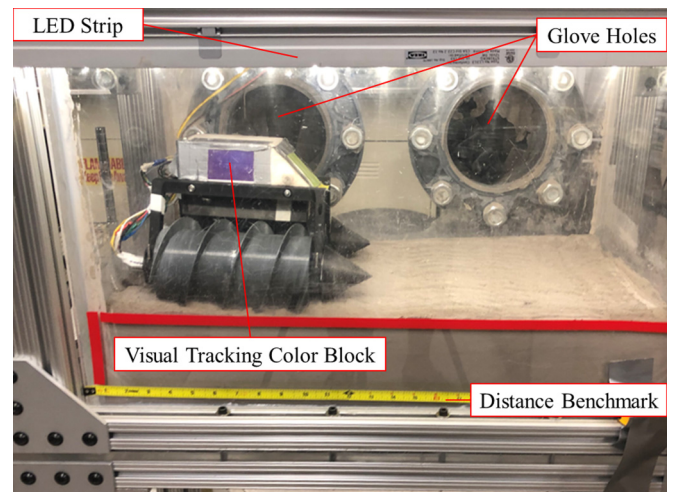

FIG. 3. Experimental setup in lunar analog chamber. The light emitting diode strip illuminates color block for position tracking.
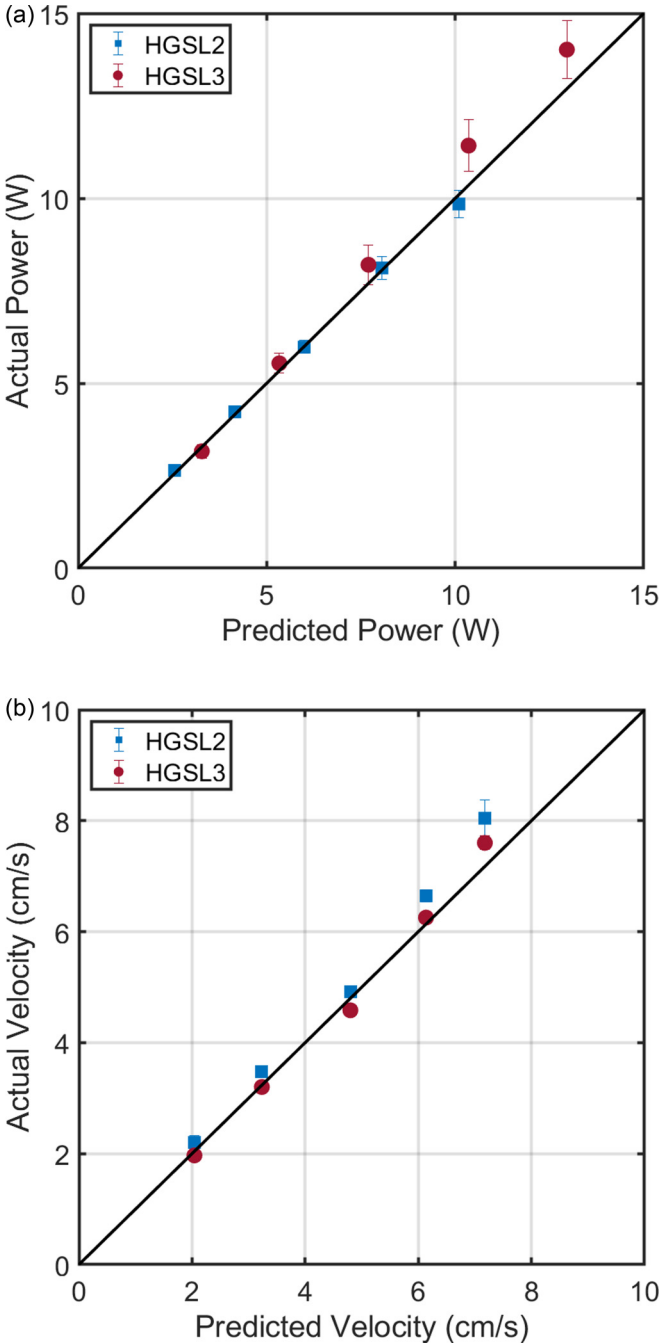
(a)

FIG. 5. Isometric view of screw pontoon vehicle in DEM parti-
cles in lunar gravity. Depth has been displayed on a warmth map with
a 4 cm difference between highest and lowest shades.

the above conditions are encouraging for the exploration of
scaling laws in other types of deformable terrains including
muds, gels, and additional simulants.

B. MBD-DEM simulations for gravity-dependent HGSL

The experiments and theory in the previous section have
been applied to only Earth terrain mechanics so far. Recall
the gravity-dependent scaling laws in Eq. (4). We retain the
scalars of a, b, relax the constraint of constant gravity, and
identify the ratio of gravities between two sets with scalar c.
Bearing in mind the need to retain a constant value for Φ, we
can perform the same procedure and constrain the necessary
variables by c,

$$\left[\frac{P}{mg\sqrt{pg}}, \frac{V}{\sqrt{pg}}\right] = \Phi\left(\frac{r_i}{p}, \frac{r_o}{p}, \frac{lp^2}{m}, \frac{g}{p\omega^2}, t\sqrt{\frac{g}{p}}\right). \quad (7)$$

This implies that the power and velocity relationships
between two sets of screws are still predictable but now
subject to a, b, c. Given the same assumptions as be-
fore, we now examine two simulation sets: One with
the inputs of $(p, m, r_i, r_o, l, \omega, g)$ and the other changed
by positive scalars a, b, c to $(p', m', r'_i, r'_o, l', \omega', g') =$
$(ap, bM, ar_i, ar_o, ba^{-2}l, a^{-1/2}c^{1/2}\omega, cg)$. The time-averaged
power and translational velocity, then, follow as

$$P' = a^{1/2}bc^{3/2}P \qquad V' = a^{1/2}c^{1/2}V. \quad (8)$$

To verify this expression, the HGSL2 and HGSL3 sizing
and mass scalars, along with a gravity scalar $c = 1/6$, were
run in a cosimulation of multibody dynamics and discrete ele-
ment method at lunar gravity (see Fig. 5) using the properties
in Table II. The results were then compared to predictions
made from an HGSL1 simulation run at Earth gravity.

We note, here, that, although the results are not directly
comparable to BP-1, all simulation parameters match that of
BP-1 or basalt as best found in the literature or by experiment.
The rolling and static friction of BP-1 on ABS and BP-1
on BP-1 were determined experimentally using modified tilt
tests and American Society for Testing and Materials (ASTM)
G194 and ASTM G219 tests. Rolling and static friction of
BP-1 on ABS were determined experimentally by spraying
spheres and a plate with adhesive, dusting with BP-1, and

(b)

FIG. 4. Time-averaged experimental results paired with their
respective predictions. The solid black line is where the model pre-
diction and experimental results are equivalent. (a) Power in units of
watts (W). (b) Velocity in units of centimeters/second (cm/s).

power to move this material. This would explain the observa-
tion of power underprediction and velocity overprediction for
some datapoints.

In general, the close agreement for velocity and power with
dimensional analysis in this experiment is a strong indicator
for the validity of HGSL for this particular material. It con-
firms that a scaling law, based on dimensional analysis, will
work for screw interactions with granular media, and a media
which displays macroscopic behaviors, such as trenching due
to strong particle friction interlock forces. Finally, both of
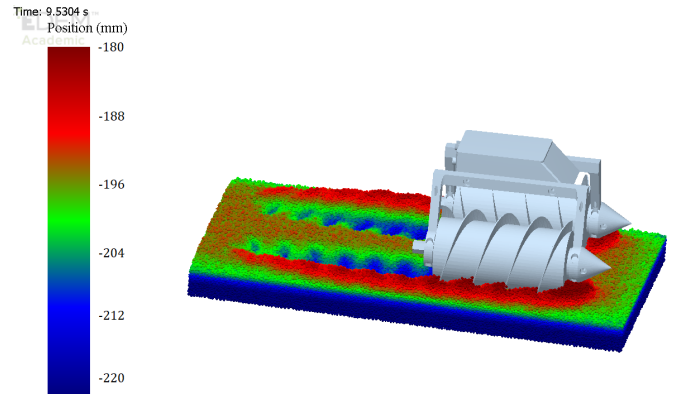
TABLE II. Properties of simulated BP-1, ABS, and interactions.

Material property	BP-1	ABS
Poisson's ratio	0.25	0.35
Density (kg/m^3)	3150	1070
Young's modulus (Pa)	73×10^7	1.8×10^9
Interactive property	BP1-BP1	BP1-ABS
Coefficient of restitution	0.8	0.8
Coefficient of static friction	0.56	0.57
Coefficient of rolling friction	0.07	0.17
Other properties	Value	
Size of bisphere clump	3 mm	
Size of tetrasphere clump	3.75 mm	
Simulation time step	9.6×10^6 s	

the experiments. Rolling and static friction of BP-1 on BP-1 were determined experimentally in a similar manner. The average from 20 tests was, then, used as the value for each. Bulk density measurements of BP-1 were taken; unconsolidated (experimental conditions) bulk density was found to be 1.561 g/cm^3, whereas consolidated density was 1.633 g/cm^3. Both of these are well within the range previously noted [31]. Young's modulus was reduced, particle size increased, and particle size normally distributed to make simulations computationally feasible. This technique has been employed before [37] for MBD-DEM vehicle dynamics and is the recommended technique for simulation acceleration [38] (see Fig. 5). These simulations would otherwise take prohibitively long to complete and, thus, this is common practice when using DEM simulations. The particles in the DEM simulation were constructed as sphere agglomerations; the granular environment is composed of 50% bisphere clumps and 50% tetrasphere clumps.

Time, power, and velocity were nondimensionalized for each corresponding Earth and lunar simulation. The average power and velocity were taken from the same dimensionless time range in steady depth for both the Earth and the lunar simulations. Figure 6 illustrates the error of −4% to 5% for all power predictions and shows a −3% to 2% error for all velocity predictions in lunar gravity simulations, predicted from Earth gravity simulations. These results, similar in error range to experiments, are better than previous MBD-DEM simulations run with wheeled craft at the same mass [29]. This is attributed to the same explanation as experiments. HGSL closely predicts the time-averaged power and velocity of screw propelled vehicles in Earth gravity experimentally and lunar gravity by simulation. These are the three-dimensional MBD-DEM simulations to examine such phenomena.

IV. CONCLUSIONS AND FUTURE DIRECTIONS

The experimental results in this paper show that a weakly cohesive silty sand with relatively small and angular particles can closely obey a scaling predictive law in a similar manner to the larger more rounded particles explored in the literature [26]. The results also show that the velocity and power of a helicoid screw shape can be predicted by HGSL provided the specified assumptions are met. Finally, simulation results show that these laws provide close prediction even when
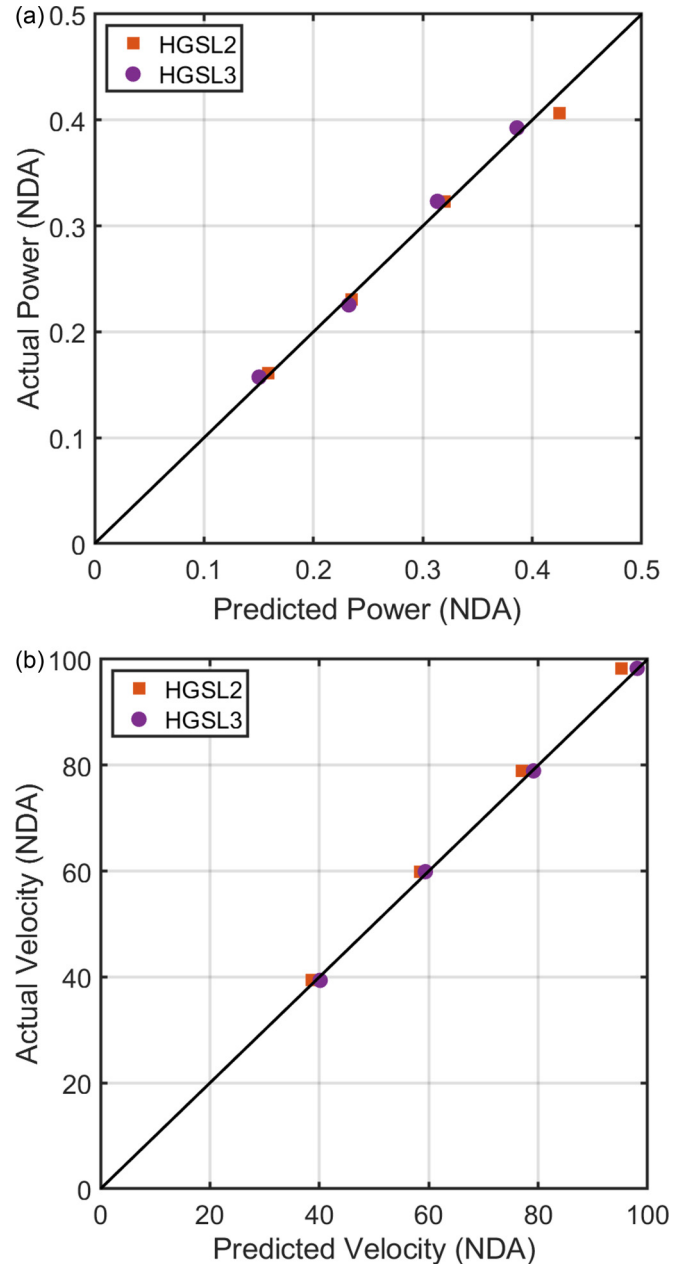

FIG. 6. The nondimensional average (NDA) results for lunar gravity simulations compared to predicted values from Earth gravity simulations. These are the time-averaged values on the left side of Eq. (7) and are unitless. The solid black line is where the model prediction and simulation results are equivalent. (a) NDA power. (b) NDA velocity.

gravity is varied, including in materials which can act as a close approximation to lunar environments. All of the above are encouraging evidence to examine dimensional analysis further in space simulants of interest. These results are also interesting for the pursuit of granular RFT in lunar or Martian simulants. Initially, it was unclear whether a granular material which deforms in the manner of BP-1 would lend itself to the RFT analysis. A paper by Askari and Kamrin [20] showed that dimensional analysis by way of the "garden hoe test" can have utility for flow models to perceive which models might

obey the RFT with discernible results. Although this is not sufficient for confirmation, the close agreement seen in the HGSL experiments, here, indicates that it is a possibility for BP-1. This contradicts the observations previously reported about using RFT for estimating forces applied on a static screw embedded in glass beads [22]. This may be because the propellerlike screw in that paper was, indeed, static and fully under the surface. Hence, the leading helices could impact the flow experienced by the trailing ones significantly more than that in a vehicle moving over the media. If other lunar or Martian simulants are characterized and shown to obey granular RFT, it would open new avenues for space vehicle testing and design. The validity of RFT for helical locomotion in BP-1 is, therefore, an interesting question worth pursuing in future papers. There is also evidence which supports expanding these scaling principles to different environments. Drag force in granular media has been shown to scale cubically with

characteristic length of some objects and a similar theoretical conclusion for colloidal matter, such as muds and soils was shown [20], providing an opportunity to explore continuum based predictions in field testing on Earth. This could include studying both screw and wheeled vehicle interactions with these deformable field environments to the benefit of certain sectors, such as agriculture or mining. There is also a question of reconciling the drag laws with continuum mobility, creating a more unified predictive model of soil and vehicle mechanics that includes both the vehicle and the tool drag. Expansion to other qualities of interest, such as drawbar pull force or tool geometry scaling dynamics could be similarly explored.

[1] M. Neumeyer and B. Jones, The marsh screw amphibian, J. Terramechanics **2**, 83 (1965).

[2] K. Evans, The history, challenges, and new developments in the management and use of bauxite residue, J. Sustainable Metallurgy **2**, 316 (2016).

[3] L. Ju, G. Ferri, C. Laschi, B. Mazzolai, and P. Dario, Experimental results of a novel amphibian solution for aquatic robot, *2010 IEEE International Conference on Robotics and Automation (ICRA)* (IEEE, Piscataway, NJ, 2010), pp. 2261–2266.

[4] A. Koshurina, M. Krasheninnikov, and R. Dorofeev, Strength calculation and analysis of equalizer beam embodiments for the operated equalizing beam suspension of the universal rotor-screw rescue vehicle for the arctic, Procedia Eng. **150**, 1263 (2016).

[5] B. D. Texier, A. Ibarra, and F. Melo, Helical Locomotion in a Granular Medium, Phys. Rev. Lett. **119**, 068003 (2017).

[6] R. Valdés, V. Angeles, E. de la Calleja, and R. Zenit, Self-propulsion of a helical swimmer in granular matter, Phys. Rev. Fluids **4**, 084302 (2019).

[7] S. Gómez, F. A. Godínez, E. Lauga, and R. Zenit, Helical propulsion in shear-thinning fluids, J. Fluid Mech. **812**, R3 (2017).

[8] N. Ho, K. Leiderman, and S. Olson, A three-dimensional model of flagellar swimming in a brinkman fluid, J. Fluid Mech. **864**, 1088 (2019).

[9] M. G. Bekker, Mechanics of locomotion and lunar surface vehicle concepts, Sae Transactions **72**, 549 (1964).

[10] M. G. Bekker, *Theory of Land Locomotion* (University of Michigan Press, Ann Arbor, MI, 1956).

[11] J. Y. Wong, *Theory of Ground Vehicles* (Wiley, Hoboken, NJ, 2008).

[12] J. Wong, Predicting the performances of rigid rover wheels on extraterrestrial surfaces based on test results obtained on earth, J. Terramechanics **49**, 49 (2012).

[13] R. D. Maladen, Y. Ding, C. Li, and D. I. Goldman, Undulatory swimming in sand: subsurface locomotion of the sandfish lizard, Science **325**, 314 (2009).

[14] R. D. Maladen, Y. Ding, P. B. Umbanhowar, A. Kamor, and D. I. Goldman, Mechanical models of sandfish locomotion

reveal principles of high performance subsurface sand-swimming, J. R. Soc., Interface **8**, 1332 (2011).

[15] Y. Ding, S. S. Sharpe, A. Masse, and D. I. Goldman, Mechanics of undulatory swimming in a frictional fluid, PLoS Comput. Biology **8**, e1002810 (2012).

[16] Y. Ding, N. Gravish, and D. I. Goldman, Drag Induced Lift in Granular Media, Phys. Rev. Lett. **106**, 028001 (2011).

[17] R. L. Hatton, Y. Ding, H. Choset, and D. I. Goldman, Geometric Visualization of Self-Propulsion in a Complex Medium, Phys. Rev. Lett. **110**, 078101 (2013).

[18] C. Li, T. Zhang, and D. I. Goldman, A terradynamics of legged locomotion on granular media, Science **339**, 1408 (2013).

[19] T. Zhang and D. I. Goldman, The effectiveness of resistive force theory in granular locomotion, Phys. Fluids **26**, 101308 (2014).

[20] H. Askari and K. Kamrin, Intrusion rheology in grains and other flowable materials, Nature Mater. **15**, 1274 (2016).

[21] S. Shrivastava, A. Karsai, Y. O. Aydin, R. Pettinger, W. Bluethmann, R. O. Ambrose, D. I. Goldman, Material re-modeling and unconventional gaits facilitate locomotion of a robophysical rover over granular terrain, Sci. Robotics **5**, eaba3499 (2020).

[22] A. Thoesen, S. Ramirez, and H. Marvi, Screw-generated forces in granular media: Experimental, computational, and analytical comparison, AIChE J. **65**, 894 (2019).

[23] K. Kamrin, Nonlinear elasto-plastic model for dense granular flow, Int. J. Plasticity **26**, 167 (2010).

[24] S. Dunatunga and K. Kamrin, Continuum modeling and simulation of granular flows through their many phases, J. Fluid Mech. **779**, 483 (2015).

[25] S. Dunatunga and K. Kamrin, Continuum modeling of projectile impact and penetration in dry granular media, J. Mech. Phys. Solids **100**, 45 (2017).

[26] J. Slonaker, D. C. Motley, Q. Zhang, S. Townsend, C. Senatore, K. Iagnemma, and K. Kamrin, General scaling relations for locomotion in granular media, Phys. Rev. E **95**, 052901 (2017).

[27] S. Agarwal, C. Senatore, T. Zhang, M. Kingsbury, K. Iagnemma, D. I. Goldman, and K. Kamrin, Modeling of the interaction of rigid wheels with dry granular media, J. Terramechanics **85**, 1 (2019).

[28] P. Jop, Y. Forterre, and O. Pouliquen, A constitutive law for dense granular flows, Nature (London) **441**, 727 (2006).

[29] A. Thoesen, T. McBryan, M. Green, J. Martia, D. Mick, and H. Marvi, Revisiting scaling laws for robotic mobility in granular media, IEEE Robotics Automat. Lett. **5**, 1319 (2020).

[30] A. Thoesen, T. McBryan, D. Mick, M. Green, J. Martia, and H. Marvi, Comparative performance of granular scaling laws for lightweight grouser wheels in sand and lunar simulant, Powder Technol. **373**, 336 (2020).

[31] E. Suescun-Florez, S. Roslyakov, M. Iskander, and M. Baamer, Geotechnical properties of BP-1 lunar regolith simulant, J. Aerospace Eng. **28**, 04014124 (2014).

[32] R. P. Mueller, R. E. Cox, T. Ebert, J. D. Smith, J. M. Schuler, and A. J. Nick, Regolith advanced surface systems operations robot (rassor), *2013 IEEE Aerospace Conference, Big Sky, MT* (IEEE, Piscataway, NJ, 2013), pp. 1–12.

[33] R. P. Mueller, Lunabotics mining competition: Inspiration through accomplishment, *Earth and Space 2012: Engineering, Science, Construction, and Operations in Challenging Environments* (American Society of Civil Engineers, Reston, VA, 2012), pp. 1478–1497.

[34] L. A. Rahmatian and P. T. Metzger, Soil test apparatus for lunar surfaces, in *Earth and Space 2010: Engineering, Science, Construction, and Operations in Challenging Environments* (American Society of Civil Engineers, Reston, VA, 2010), pp. 239–253.

[35] I. Townsend, A. C. Muscatello, D. Dickson, L. Sibille, A. Nick, K. Leucht, and G. Tamasy, Mars isru pathfinder regolith autonomous operations-modeling and systems integration, *AIAA SPACE and Astronautics Forum and Exposition, Orlando, FL, 2017* (AIAA, Reston, VA, 2017), p. 5150.

[36] M. Heverly, J. Matthews, J. Lin, D. Fuller, M. Maimone, J. Biesiadecki, and J. Leichty, Traverse performance characterization for the mars science laboratory rover, J. Field Robotics **30**, 835 (2013).

[37] A. Thoesen, T. McBryan, and H. Marvi, Helically-driven granular mobility and gravity-variant scaling relations, RSC Adv. **9**, 12572 (2019).

[38] S. Lommen, D. Schott, and G. Lodewijks, Dem speedup: Stiffness effects on behavior of bulk material, Particuology **12**, 107 (2014).